SUPPLEMENTARY MATERIAL

Device assembly

The PDMS transducer was thoroughly cleaned then placed into the aligner as shown in Figure S1. The ensemble underwent air plasma treatment at 45 W for 30s (AutoGlow Plasma System, Glow Research), along with the post-NPN channel mold. After plasma, the molds were lined up using the alignment posts and pressed firmly together for 30s, then placed in 70°C oven for 40 minutes. Once cured, 0.75 mm biopsy punches were subsequently used to punch holes for fluidic access to the transducer layer.

At the time of assembly, the chips were placed etch pit side down on the chip stand. The chip guide was aligned and lowered over the chip stand. The pre-NPN PDMS components were placed in the top jig which was aligned over the chip via the alignment posts on the chip guide. Subsequent to alignment, the entire assembly was inverted to facilitate the removal of the chip stand and chip guide. The gasket was placed around the chip to ensure proper alignment and to prevent leakage of fluid during the subsequent testing phases. Post-NPN PDMS components were loaded into the post-NPN alignment jig and aligned with the chip using the alignment posts. The device was interposed between 2 acrylic clamping layers with cutouts to allow for fluidic access. The acrylic components were designed in Onshape and imported into LaserCut 5.3 (HPC Laser). Parts were cut from 3 mm thick acrylic using the JAMIESON LASER LG-500 cutter. In order to prevent leakage, force was evenly distributed over the entire assembly by adjusting the tightness of nuts and bolts stationed at the four corners of the assembly.

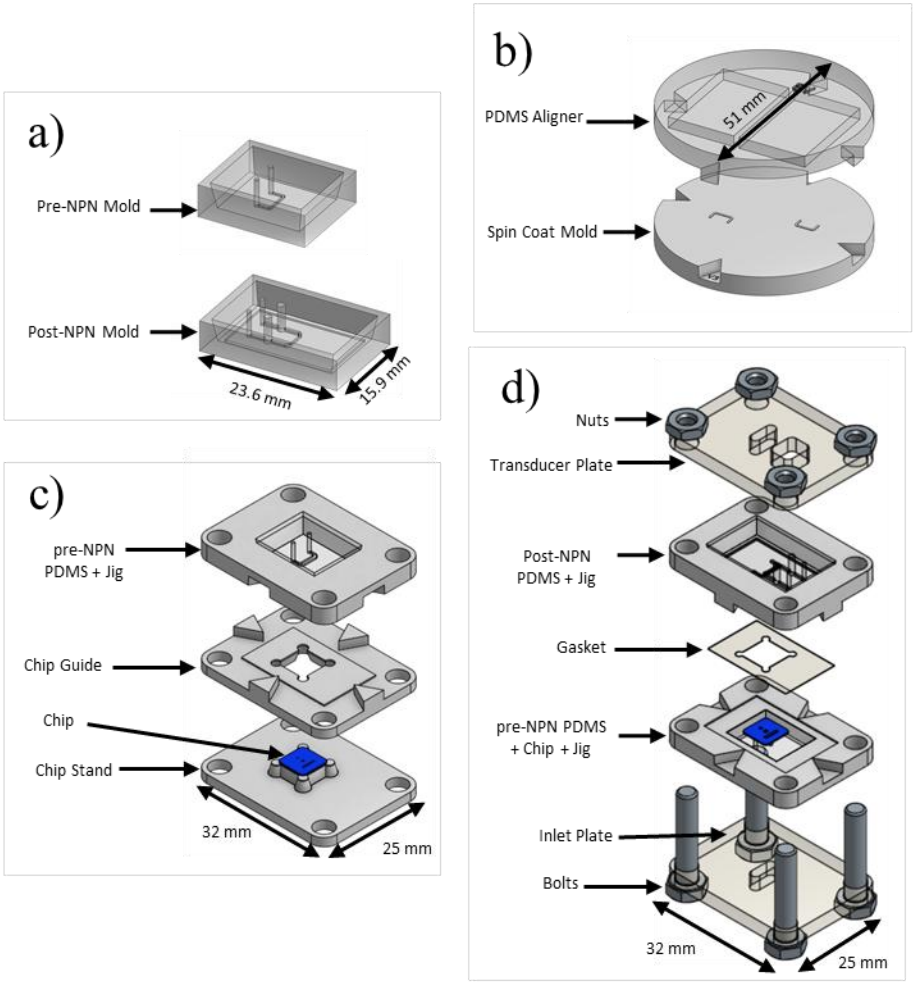

Figure S1. Component list and assembly diagram of the proposed microfluidic device (a) 3D printed molds for curing of bulk PDMS components, (b) 3D printed components for membrane spin coating and alignment, (c) Alignment components for between on chip NPN and fluidic access channels. (d) Exploded view of complete device assembly.

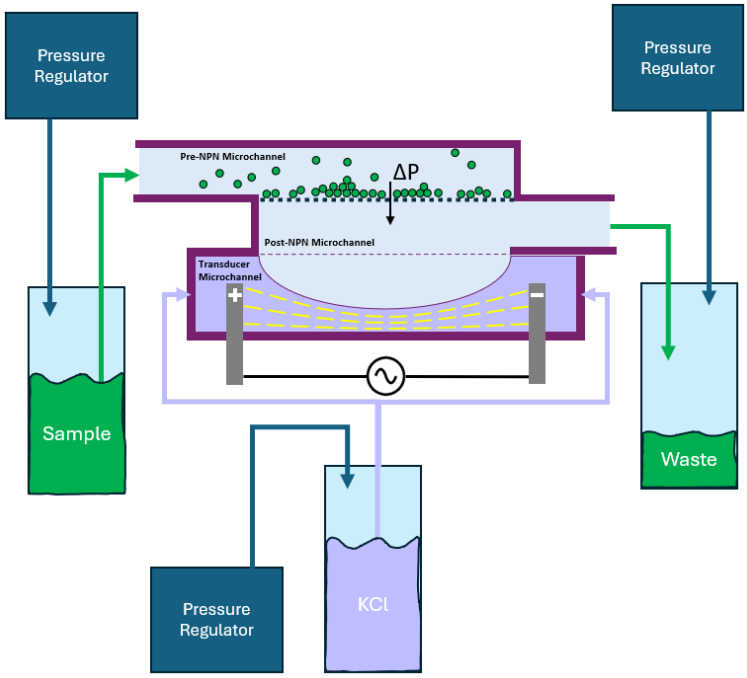

Fluidic Setup

Fig.S2: Fluid delivery system and pressure control: The system must be pressurized in order for the transducer to properly function and for the nanoparticles to be successfully captured by the NPN. Pressures of the vials are modulated via the use of SMC ITV1011-311N digital pressure regulators controlled by a custom LabVIEW testing program. The pressure at the inlet and outlet of the NPN channel must be individually controlled to allow for the introduction of pressure gradients within the system in order to initiate particle flow. Pressure within the transducer microchannel must remain constant throughout the experiment and is therefore controlled using a dedicated pressure regulator.

Membrane Properties:

To confirm that the NPN is successfully capturing the nanoparticles, a sample containing europium chelate fluorescently tagged beads was passed through the device. Images were taken before and after flow to confirm the membrane was successfully fouled (Fig S3). Fluorescent spots on the membrane being observable only post introduction of the nanoparticles indicates that they were successfully captured by the NPN. The presence of locally bright and dim areas indicates that uneven particle deposition is occurring across the NPN as pore blockage and particle caking are not uniform and easily replicable processes. Initial particle deposition sites and subsequent particle caking is determined via a variety of initial system factors including the configuration of the fluidic pathway, particle/ sample velocity, and Renold's number[1].

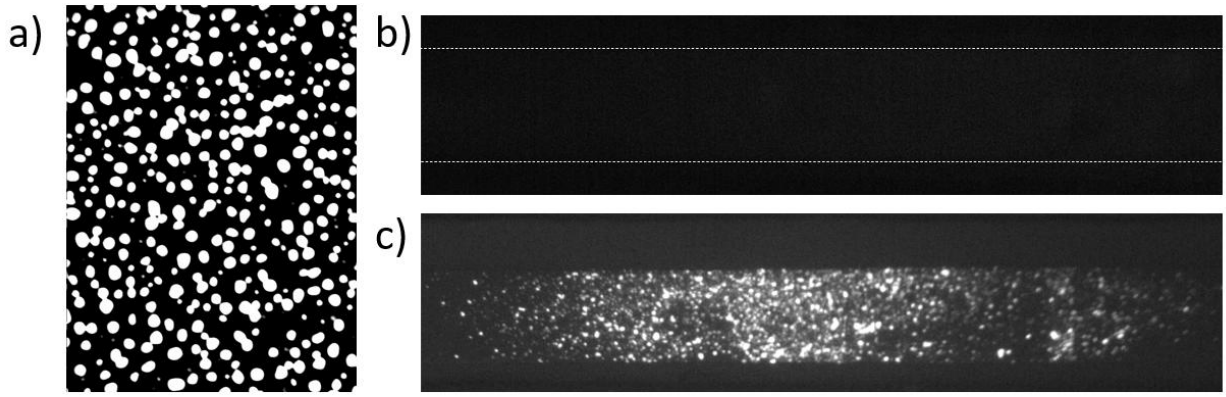

Fig.S3: Membrane properties and fouling with fluorescently tagged particles: (a) TEM image of the NPN membrane surface. To confirm the membrane is fouling, a sample containing europium chelate tagged polystyrene particles were passed through the device. Fluorescent images of the NPN membrane were taken (b) before (membrane outlined) and (c) following sample flow.

Effect of NPN Wetting on Blocking and Caking Efficiencies

NPNs are delivered completely dry meaning that the pores of the membrane are saturated with air. To allow for proper flow across the NPN, the sample solution must overcome the vapor pressure of air trapped within the pores[2] in a process termed "pore wetting". If a pore is not wet, the sample is not able

to flow through it, meaning that the initial number of functional pores to block is reduced. This reduction in functional pores changes the initial conditions of the system and can influence the overall pressure change kinetics of the system. The wetting efficiency represents the percentage of total pores sufficiently wet as to allow for trans-membrane flow of the sample. Using our computational model, simulations were generated to evaluate the effect of the wetting efficiency on the pressure response curve. To study the combined effect of the wetting and blocking efficiencies, the simulations were generated for a system at 10% blocking efficiency (Figure S4 a), 50% blocking efficiency (Figure S4 b), and 100% blocking efficiency (Figure S4 c), respectively, while varying the wetting efficiency in increments of 20% in the range of 20-100% of the total pores wet for each set blocking efficiency. The pressure response curve is dependent on the initial wetting efficiency of the NPN membrane. As the wetting efficiency is increased, the pressure at time zero increases and the observed pressure trend over time visibly changes. As wetting efficiency decreases, the pressure response plateau will decrease as well. However, the decrease in plateau and change in pressure response is less observable as blocking efficiency of the system increases.

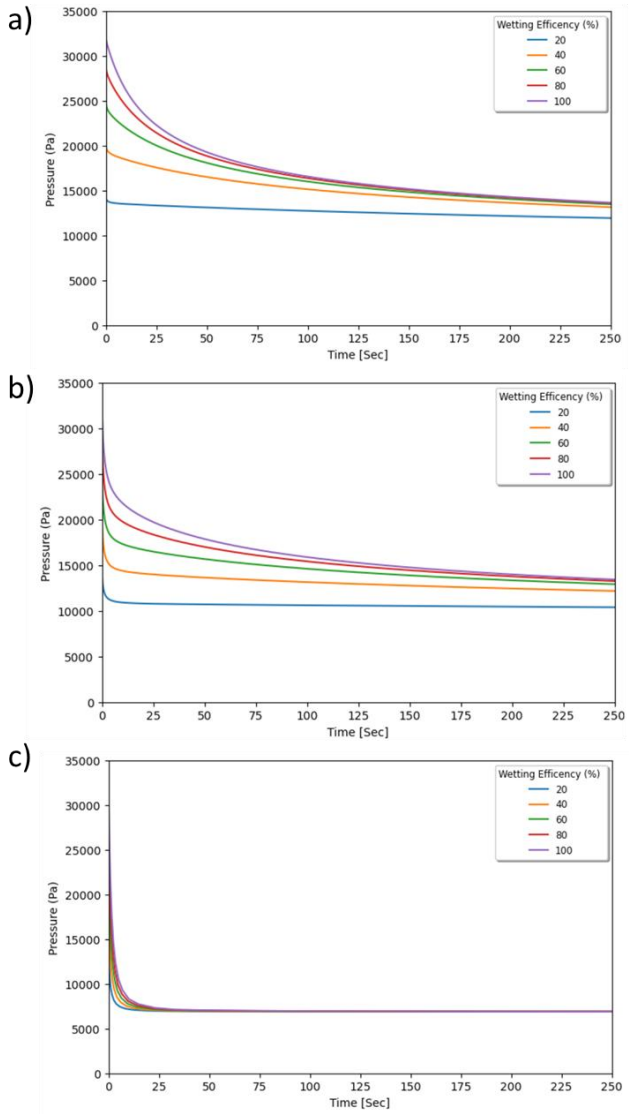

Figure S4. Wetting Efficiency: During device priming, solution must penetrate the pores of the NPN and displace air in a process termed "pore wetting". When a part of the NPN is not properly wet, it is not possible for sample to flow through the membrane at the given pores. Wetting efficiency represents the percent of pores wet and therefore accessible for flow across the NPN. (a) Simulated pressure response over time for varying wetting efficiencies at 10% blocking efficiency. (b) Simulated pressure response over time for varying wetting efficiencies at 50% blocking efficiency. (c) Simulated pressure response over time for varying wetting efficiencies at 100% blocking efficiency.

Modeling parameters

The conceptual framework of membrane blockage used in this work was adapted from existing classical models of membrane fouling[3–5], though a different approach was taken for the mathematical description of this process. The classical models of membrane fouling, generally applicable under constant pressure or constant flow rate conditions, address four primary blockage modes: complete blocking, standard blocking, intermediate blocking, and cake filtration. The model presented in this report seeks to describe cake filtration, as well as a modified version of complete blocking, here referred to as partial blocking, where particles may partially block a pore, thus reducing the flow according to a certain 'blocking efficiency', representative of flow reduction through a given pore, valued between 0 and 1. These two blockage modes are applicable in the case where particle sizes are equivalent to or larger than the membrane's pore size. This model is applicable in the case of variable pressure and flow rate, as required by the experimental procedure used for pressure measurements in the system.

The three constants related to particle caking, these being minimum and maximum packing density δ_{min} and δ_{max} respectively, and the characteristic flow rate q, were difficult to measure directly and were therefore treated as fitting parameters. Approximate minimum and maximum packing densities could be intuited by treating the caking layer as a case of sphere packing. Assuming maximum packing density corresponds to a tight random sphere packing with $\delta_{max} = 0.64$ and minimum packing density corresponds to a very loose sphere deposition with $\delta_{min} \leq 0.55$ generally provides acceptable results[6]. The characteristic flow rate determines the transition from tight to loose packing and can be adjusted globally according to experimental observations. Given a function with n variables, an initial "simplex" is chosen with n+1 initial points, meaning in this case the initial simplex will be of the form $\{-R^2(c_0, b_0), -R^2(c_1, b_1), -R^2(c_2, b_2)\}$. From this initial simplex, the algorithm will converge towards a value which minimizes the function. The value to which the algorithm converges can be sensitive to this choice of initial simplex, and convergence towards a global minimum is not always guaranteed due to the

presence of local minima. However, it is usually clear when the algorithm has converged to a non-optimal value.

Caking Resistance

Consider a layer of n_{pc} particles that have deposited onto the membrane. The particles may be considered as roughly spherical, forming a porous volume of packed spheres. The resistance of this layer can be described by Darcy's law for flow through porous mediums, given by:

$$R = \frac{\mu h}{kA},$$

where $\mu \in \mathbb{R}_+$ is the fluid dynamic viscosity, $h \in \mathbb{R}_+$ is the layer height, $k \in \mathbb{R}_+$ is a permeability factor, and $A \in \mathbb{R}_+$ is the cross-sectional area of the membrane.[7,8] The permeability will vary according to a function $k(z): \mathbb{R}_+ \longrightarrow \mathbb{R}_+$ which describes the permeability k as a function of vertical position in the caking layer z. The height will also increase over time as particles continue to be deposited, described by the function $h(t): \mathbb{R}_+ \longrightarrow \mathbb{R}_+$. The equation for caking layer resistance then becomes:

$$R_c(t) = \int_0^{h(t)} \frac{\mu}{k(z)A} dz.$$

Caking Growth

To determine the change in height over time, the change in height as a function of caked particles can first be determined, then combined with the change in deposited particles over time such that

$$\frac{dh}{dt} = \frac{dh}{dn_{pc}} \cdot \frac{dn_{pc}}{dt}.$$

The caking volume can be split into solid particle volume V_p and void volume V_v giving

$$\Delta V = \Delta V_p + \Delta V_v.$$

The change in volume of solid particles will be the sum of the volumes of every individual newly deposited particle, which, assuming spherical particles, is given by

$$\Delta V_p = \sum_{j=0}^{\Delta n_{pc}} \frac{1}{6}\pi y_j^3 = \Delta n_{pc} \cdot \frac{\pi}{6} \cdot E[y^3],$$

where y_j is a random variable from the particle diameter distribution $G(y)$, and $E[y^3]$ is the expectation value of y^3. The particles will deposit with some packing density $\delta(t)$: $\mathbb{R}_+ \longrightarrow [0,1]$ which is allowed to vary as a function of time. Note that $\delta(t)$ represents the packing density at which particles are being deposited. Once a layer of particles is deposited at a time t_0, it is assumed that it maintains a constant packing density $\delta(t_0)$. The packing density is defined by

$$\delta = \frac{V_p}{V}.$$

The change in height is therefore given by

$$\Delta h = \frac{\Delta V}{A} = \Delta n_{pc} \cdot \frac{\pi}{6A} \cdot E[y^3] \cdot \frac{1}{\delta(t)}.$$

Where ΔV is the finite difference in caking volume. In differential form, the change in height over time:

$$\frac{dh}{dt} = \frac{\pi}{6A} \cdot E[y^3] \cdot \frac{1}{\delta(t)} \cdot \frac{dn_{pc}}{dt}.$$

Permeability

Moving to the description of the permeability function $k(z)$, an expression to describe the permeability of a thin layer of particles is needed. Similarly to existing models[5] of cake filtration, the Kozeny-Carman equation[9] is used, given by

$$k = \Phi_s^2 \cdot \frac{(1-\delta)^3 d_p^2}{180\delta^2},$$

where Φ_s is the sphericity of the particles, taken here to be 1, and d_p is the diameter of the volume equivalent spherical particle, meaning the diameter of a spherical particle with a volume equivalent to the mean volume of the full particle distribution. This is given by

$$d_p = E[y^3]^{\frac{1}{3}}.$$

Substituting these into the Kozeny-Carman equation gives

$k = \frac{(1-\delta)^3 \cdot E[y^3]^{\frac{2}{3}}}{180 \cdot \delta^2}$.

To determine $k(z)$, the packing density as a function of vertical position in the caking layer $\delta(z)$: $\mathbb{R}_+ \longrightarrow [0,1]$ will first need to be determined. For a given packing density as a function of time $\delta(t)$ and layer height as a function of time $h(t)$, the inverse layer height function $h^{-1}(z)$: $\mathbb{R}_+ \longrightarrow \mathbb{R}_+$ may be used to determine the time t at which $h(t) = z$. This means that the packing density as a function of vertical position is given by:

$\delta(z) = \delta(t) \circ h^{-1}(z)$,

And the permeability function may be written as

$k(z) = \frac{E[y^3]^{\frac{2}{3}}}{180} \cdot \frac{(1-\delta[h^{-1}(z)])^3}{\delta[h^{-1}(z)]^2}$.

The caking resistance function can then be given by:

$$R_c(t) = \frac{180\mu}{E[y^3]^{\frac{2}{3}}A} \cdot \int_0^{h(t)} \frac{\delta[h^{-1}(z)]^2}{(1-\delta[h^{-1}(z)])^3} dz$$

Deposition Density

To fully define the caking resistance, we need to determine the packing density function $\delta(t)$. We'll assume that the caking layer can be described as a bed of randomly packed spherical particles. Unfortunately, the exact packing behavior of particles under a fluid flow is complex to derive and beyond the scope of this project, but we can make some approximations and assumptions that will allow us to get a stand in function that can reasonably approximate the expected behavior. The density of the packed particles should be dependent on the force acting to compress them. In this case, the force compressing the particles is induced by the movement of the fluid through the system, meaning the packing density

should be in some way dependent on flow rate. We'll define $\delta(Q)$: $\mathbb{R}_+ \longrightarrow [0,1]$ the packing density as a function of flow rate, and define our density as a function of time as

$$\delta(t) = \delta(Q) \circ Q(t)$$

The density of the particle deposition, assuming random packing, should have a certain maximum possible value $\delta_{max} \epsilon [0,1]$, at which point it is impossible to achieve tighter packing. There should also be some minimum possible packing density $\delta_{min} \epsilon [0,1]$, at which point, assuming particles are still being added to the system, it is impossible to achieve a looser deposition packing. δ_{max} should be the least upper bound of $\delta(Q)$ and should be achieved when the compression force on the particles is the highest, and δ_{min} should be the greatest lower bound of $\delta(Q)$ and should be achieved when compression force on the particles is the lowest.

We'll also assume that the function $\delta(Q)$ is an increasing function, since an increase in flow rate should result in an increase in packing density. Our choice for $\delta(Q)$ must satisfy all the above conditions. We'll choose an inverse exponential function, defining the packing density function as a function of time, defined as

$$\delta(t) = (\delta_{max} - \delta_{min}) \cdot \left(1 - e^{-\frac{1}{q}Q(t)}\right) + \delta_{min}.$$

where e is Euler's number and q is some characteristic flow rate. It can be shown that this function satisfies all the above conditions. The choice of the function is otherwise mostly arbitrary, but it is one of the simplest functions which meets our desired criteria and as such should work as a stand in function to approximate the packing density behavior. Leaving q as a simple parameter means that we have all we need to fully describe the system's caking behavior.

Error analysis

Bootstrapping analysis was utilized to determine the uncertainty of the fitting algorithm. The process involves resampling data points by random selection.[10] 6 data points were randomly sampled from the original set of 6 points per iteration, allowing for the repetition of time-points. Each resampled data set was fed to the Nelder-Mead multivariable optimizer for predictive analysis. By resampling and refitting 15 000 times, a distribution of predicted concentrations was obtained, an example of which can be observed in fig s5. The spread of the predicted concentrations obtained via bootstrap analysis was used to construct the confidence intervals of the predictive model. Since individual data point uncertainties were not considered in the fitting, the bootstrap analysis was utilized only to determine variability of fit due to a finite sample size and accuracy of the physics model rather than uncertainty due to measurement error of the integrated pressure transducer. The variability of predicted concentrations, and by extension the confidence intervals of the model's prediction, are unique among experimental runs, indicating a bootstrap analysis must be completed for each test. Cloud-based computing via the Digital Research Alliance of Canada (DRAC) was utilized to accommodate the computational expense of bootstrapping.

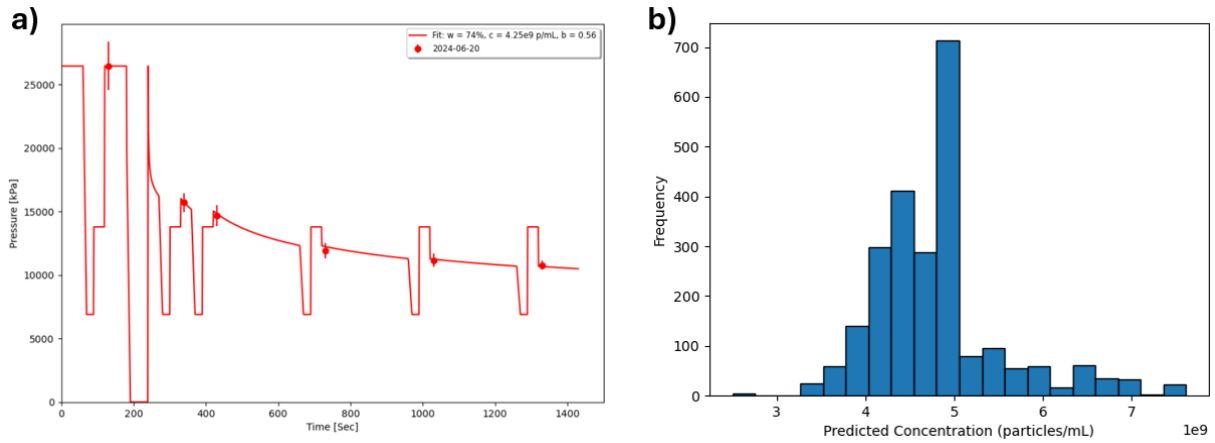

Figure S5. Predictive model fitting. (a) Predictive analysis for a 4.9x10^{9} particles/mL sample. Sample concentration was predicted to be 4.3x10^{9} particles/mL. (b) Bootstrapping analysis of the same set of experimental data. The average predicted concentration of the bootstrap analysis was determined to be 4.8 x10^{9} particles/mL with a standard deviation of the predicted concentrations of 0.7 x10^{9} particles/mL

WORKS CITED:

1. Kwak, D.-B., Kim, S. C., Lee, H. & Pui, D. Y. H. Numerical investigation of nanoparticle deposition location and pattern on a sharp-bent tube wall. *International Journal of Heat and Mass Transfer* **164**, 120534 (2021).
2. Chen, Y., Wang, Z., Jennings, G. K. & Lin, S. Probing Pore Wetting in Membrane Distillation Using Impedance: Early Detection and Mechanism of Surfactant-Induced Wetting. *Environ. Sci. Technol. Lett.* **4**, 505–510 (2017).
3. Iritani, E. & Katagiri, N. Developments of Blocking Filtration Model in Membrane Filtration. *KONA Powder and Particle Journal* **33**, 179–202 (2016).
4. Iritani, E. A Review on Modeling of Pore-Blocking Behaviors of Membranes During Pressurized Membrane Filtration. *Drying Technology* **31**, 146–162 (2013).
5. Sanaei, P. & Cummings, L. J. Membrane filtration with multiple fouling mechanisms. *Phys. Rev. Fluids* **4**, (2019).
6. Song, C., Wang, P. & Makse, H. A. A phase diagram for jammed matter. *Nature* **453**, 629–632 (2008).
7. Macciotta, R. Darcy's Law. in *Encyclopedia of Engineering Geology* (eds Bobrowsky, P. T. & Marker, B.) 205–206 (Springer International Publishing, Cham, 2018). doi:10.1007/978-3-319-73568-9_79.
8. Basic theory. in *Fluid Flow in Porous Media* 47–67 (WORLD SCIENTIFIC, 2020). doi:10.1142/9789811219535_0002.
9. Kruczek, B. Carman–Kozeny Equation. in *Encyclopedia of Membranes* (eds Drioli, E. & Giorno, L.) 1–3 (Springer, Berlin, Heidelberg, 2015). doi:10.1007/978-3-642-40872-4_1995-1.
10. Efron, B. & Tibshirani, R. The Bootstrap Method for Assessing Statistical Accuracy. *Behaviormetrika* **12**, 1–35 (1985).